Galvanomagnetic Effects in Antimony at Liquid-Helium Temperatures*

G. N. Rao,† N. H. Zebouni, C. G. Grenier, and J. M. Reynolds
Department of Physics, Louisiana State University, Baton Rouge, Louisiana
(Received 21 August 1963)

Galvanomagnetic effects in a single crystal of antimony were studied at liquid-helium temperatures in magnetic fields up to 18 kG. A study of the Shubnikov-de Haas oscillations with respect to crystal orientation was made to map the Fermi surfaces of the carriers. The electron Fermi surface was found to agree with the tilted ellipsoid model proposed by Shoenberg. The hole Fermi surface could not be determined unambiguously; the data were found to be compatible with a three-ellipsoid model. The nonoscillatory parts of the conductivities were analyzed on the basis of the Sondheimer–Wilson theory in the two-band model. The results showed an equal number of electrons and holes with the mobilities of the electrons being five times larger than that of the holes. The amplitudes of the oscillations in the conductivities were found to disagree with the Lifshitz–Kosevich theory but to agree (magnetoconductivity only) in order of magnitude with the Zil'berman theory.

I. INTRODUCTION

A COMPLETE study of the transport properties of a metal requires the experimental determination of a set of transport coefficients from which the elements of the electrical conductivity tensor, the thermal conductivity tensor and the thermoelectric tensor can be computed.[1–3] The present paper reports measurements and analyses of galvanomagnetic effects as the first part of such a study of antimony.

Investigations made to determine the band structure of antimony include studies of the de Haas–van Alphen effect,[4] of cyclotron resonance,[5,6] of ultrasonic attenuation,[7,8] of the Shubnikov-de Haas effect,[9] and of galvanomagnetic effects both at room-temperature[10,11] and at liquid-helium temperatures.[12] Experimental results[4,10,11] indicate a carrier density of the order of 10^{-3} per atom. Theoretical considerations[13] show that the Fermi surfaces for such low carrier densities are nearly ellipsoidal.

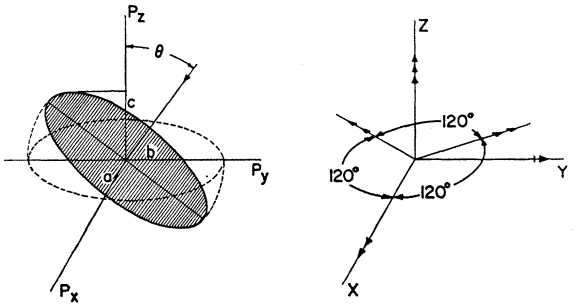

FIG. 1. Tilted ellipsoid model for electrons. The angle of tilt being 36°.

A model for the electron part of the Fermi surface was first established experimentally from the de Haas-van Alphen oscillations.[4] The electron Fermi surfaces consist of three ellipsoids in momentum space with their centers lying on the binary axes in the basal (1–2) plane as shown in Fig. 1. Each ellipsoid is tilted by an angle 36° out of the basal plane toward the trigonal axis. Figure 2 defines the coordinate system with respect to the crystal axes.

An indication of the existence of holes was found by Datars,[6] Ketterson,[8] and Epstein[11] but the exact shape of the Fermi surfaces for holes is still uncertain. In the present work, both electrons and holes were found. The data are interpreted on the basis of the usual set of three ellipsoids for electrons. Two alternative interpretations are proposed for the holes, first, three ellipsoid Fermi surfaces analogous to the electron ellipsoids and second, a two-hole band model.

The galvanomagnetic effects in antimony measured at liquid-helium temperatures were analyzed on the basis of present theories. The oscillations in magneto-

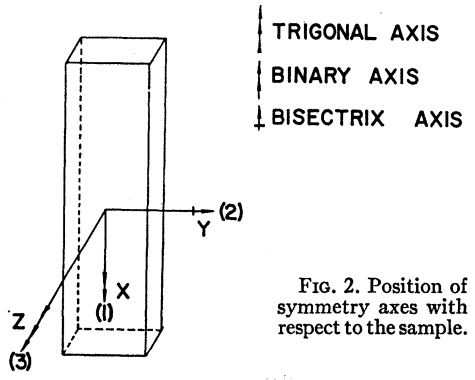

FIG. 2. Position of symmetry axes with respect to the sample.

* This work was supported by the U. S. Atomic Energy Commission.
† Part of this work was submitted (by G.N.R.) in partial fulfillment of the requirements for the Ph.D. degree at Louisiana State University.

[1] H. B. Callen, Phys. Rev. 85, 16 (1952).
[2] P. Mazur and I. Prigogine, J. Phys. Radium 12, 616 (1951).
[3] C. G. Grenier, J. M. Reynolds, and N. H. Zebouni, Phys. Rev. 129, 1088 (1963).
[4] D. Shoenberg, Phil. Trans. Roy. Soc. London A245, 1 (1952).
[5] W. R. Datars and R. N. Dexter, Phys. Rev. 124, 75 (1961).
[6] W. R. Datars, Can. J. Phys. 39, 1922 (1961).
[7] Y. Eckstein, Phys. Rev. 129, 12 (1963).
[8] J. B. Ketterson, Phys. Rev. 129, 18 (1963).
[9] J. Ketterson and Y. Eckstein, Bull. Am. Phys. Soc. 8, 548 (1962).
[10] S. J. Freedman and H. J. Juretschke, Phys. Rev. 124, 1379 (1961).
[11] S. Epstein and H. J. Juretschke, Phys. Rev. 129, 1148 (1963).
[12] M. C. Steele, Phys. Rev. 99, 1751 (1955).
[13] M. H. Cohen, Phys. Rev. 121, 387 (1961).

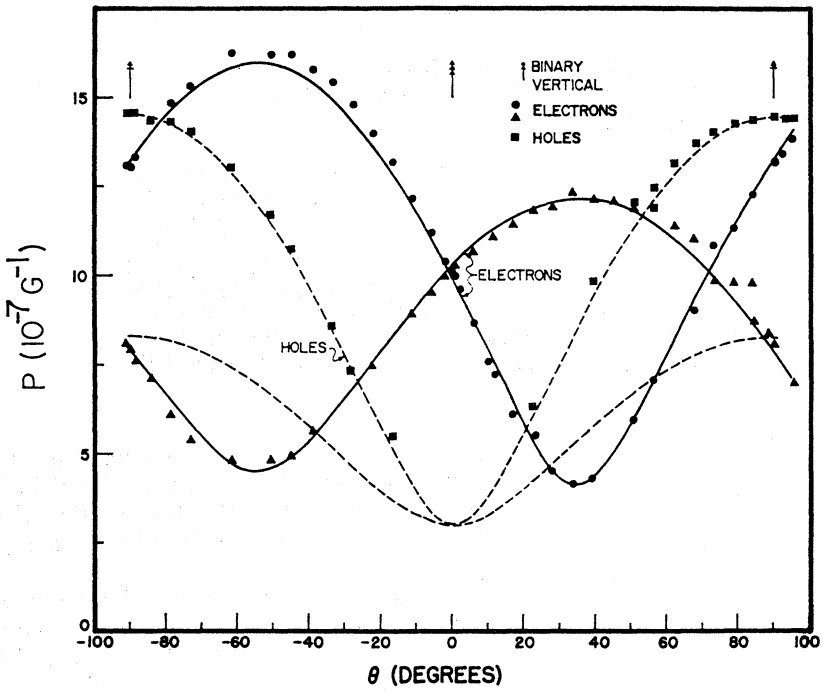

FIG. 3. Period P versus angle θ where P is the oscillation period with the binary axis normal to H and θ the angle between the trigonal axis and H. The curves are the least-squares fit of Eq. (6).

resistance were decomposed into Shubnikov-de Haas oscillations, periodic in $1/H$. The periods of these oscillations at different orientations of the crystal with respect to the magnetic field were interpreted to determine the Fermi surfaces for the carriers in the metal, Sec. II. The gross effects upon which the oscillations superimpose were analyzed on the basis of the Sondheimer-Wilson theory in the two-band model, Sec. III. The oscillations in the conductivities are discussed in Sec. IV.

Details and references to additional detailed information on the experimental sample, arrangements, and techniques are given in the Appendix.

II. STUDY OF THE DEPENDENCE OF THE SHUBNIKOV-DE HAAS EFFECT ON CRYSTAL ORIENTATION

A. Experimental Results

The equation of a tilted ellipsoidal Fermi surface segment in momentum space with the center of the ellipsoid taken as the origin of the coordinate system is

$$\alpha_{11}p_1^2+\alpha_{22}p_2^2+\alpha_{33}p_3^2+2\alpha_{23}p_2p_3=2m_0\zeta_0, \quad (1)$$

where the subscripts 1, 2, 3 refer to binary, bisectrix and trigonal directions, respectively; ζ_0 is the chemical potential of the carriers, and m_0 is the mass of the free electron. The α's are the elements of the tensor $\hat{\alpha}=m_0\hat{m}^{*-1}$, where $\hat{m}^{*-1}$ is the inverse effective mass tensor; $\hat{\alpha}$ has the form

$$\hat{\alpha}=\begin{bmatrix}\alpha_{11} & 0 & 0\\ 0 & \alpha_{22} & \alpha_{23}\\ 0 & \alpha_{23} & \alpha_{33}\end{bmatrix}. \quad (2)$$

The other two ellipsoids of the three ellipsoid set are obtained by rotation of Eq. (1) through $\pm 120°$ about the trigonal axis.

The Shubnikov-de Haas oscillations are analyzed into components, each component periodic in $1/H$. The period of each component is given in terms of an extremal area S_m of a planar cross section of the Fermi surface

$$P=eh/cS_m, \quad (3)$$

where the planar area S_m is perpendicular to the magnetic field direction. The area S_m for the ellipsoid of Eq. (1) is written in polar coordinates; the period P is then expressed as

$$P^2=[A\cos^2\theta+B(\sin^2\psi+C\cos^2\psi)\sin^2\theta - 2D\sin\theta\cos\theta\sin\psi] \quad (4)$$

where

$$\begin{aligned} A&=(eh/2m_0c\zeta_0)^2\alpha_{11}\alpha_{22},\\ B&=(eh/2m_0c\zeta_0)^2\alpha_{11}\alpha_{33},\\ C&=(eh/2m_0c\zeta_0)^2(\alpha_{22}\alpha_{33}-\alpha_{33}^2),\\ D&=(eh/2m_0c\zeta_0)^2\alpha_{11}\alpha_{23}, \end{aligned} \quad (5)$$

θ is the angle between the magnetic field and the trigonal axis, and ψ is the azimuthal angle. The two other ellipsoids give rise to periods with similar expressions in which ψ is replaced by $\psi\pm 120°$.

Experiments were performed with the field orientation in three different crystallographic planes. The crystal was placed in the cryostat in the following positions:

(i) With the binary axis vertical so that H horizontal

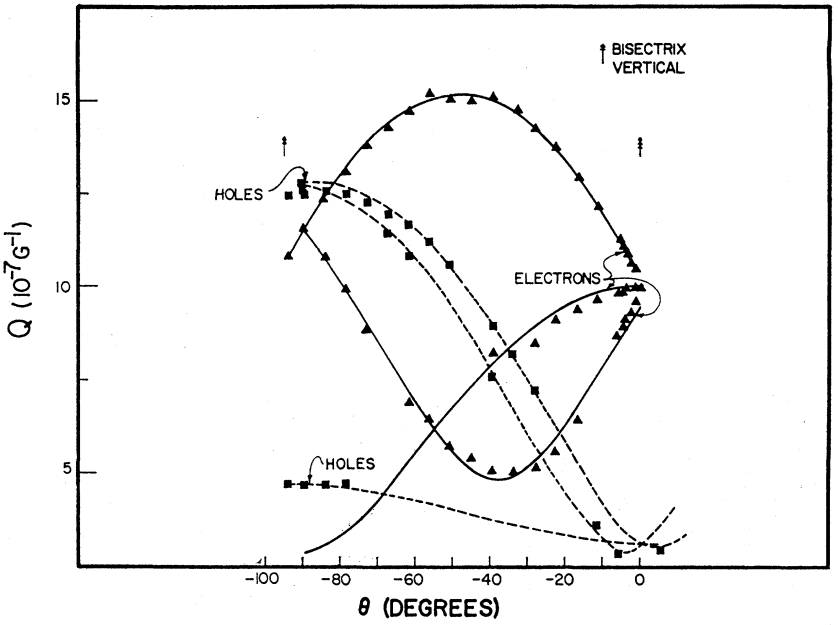

FIG. 4. Period Q versus angle θ where Q is the period of the oscillation in $1/H$ with the bisectrix axis normal to H and θ the angle between the trigonal axis and H. The curves are the least-squares fit of Eq. (7).

was in the (2–3) plane, Eq. (4) reduces in this case to

$$\begin{aligned}
&\psi=90°, \quad P_1^2=A\cos^2\theta+B\sin^2\theta-2D\sin\theta\cos\theta;\\
&\psi=210°, \quad P_2^2=A\cos^2\theta+\tfrac{1}{4}(B+3C)\sin^2\theta\\
&\qquad\qquad +D\sin\theta\cos\theta; \quad (6)\\
&\psi=-30°, \quad P_3^2=P_2^2;
\end{aligned}$$

where P_1, P_2, P_3 are the periods corresponding to the three ellipsoids. The data for the P's are given in Fig. 3.

(ii) With the bisectrix vertical and the field in (1–3) plane, Eq. (4) becomes

$$\begin{aligned}
&\psi=0, \quad Q_1^2=A\cos^2\theta+C\sin^2\theta;\\
&\psi=120°, \quad Q_2^2=A\cos^2\theta+\tfrac{1}{4}(3B+C)\sin^2\theta\\
&\qquad\qquad +\sqrt{3}D\sin\theta\cos\theta; \quad (7)\\
&\psi=-120°, \quad Q_3^2=A\cos^2\theta+\tfrac{1}{4}(3B+C)\sin^2\theta\\
&\qquad\qquad -\sqrt{3}D\sin\theta\cos\theta;
\end{aligned}$$

where Q_1, Q_2, and Q_3 are the periods of the three ellipsoids under condition (ii). The data for the Q's are given in Fig. 4.

(iii) With the trigonal axis vertical and the field in (1–2) plane, Eq. (4) is

$$\begin{aligned}
&R_1^2=B\sin^2\psi+C\cos^2\psi;\\
&R_2^2=B\sin^2(\psi+120)+C\cos^2(\psi+120); \quad (8)\\
&R_3^2=B\sin^2(\psi-120)+C\cos^2(\psi-120);
\end{aligned}$$

where the periods here are denoted by R_1, R_2, and R_3. The data for the R's are given in Fig. 5.

The above nine equations for the periods were used for the determination of A, B, C, and D from the experimental data. The values were obtained as the weighted average of values determined for each curve by least-square fitting to the curve, the weighting being proportional to the number of data for the curve. The period for the holes at $\theta=0$, case (i) and Fig. 3, and the periods for the electrons at $\theta=-90°$, case (ii) and Fig. 4, and at $\psi=0°$, case (iii) and Fig. 5, were either too small to observe or too complicated to analyze. The parameter C presented some difficulty. Values for C were obtained as the $\psi=0$ intercepts of straight lines fitted to the R

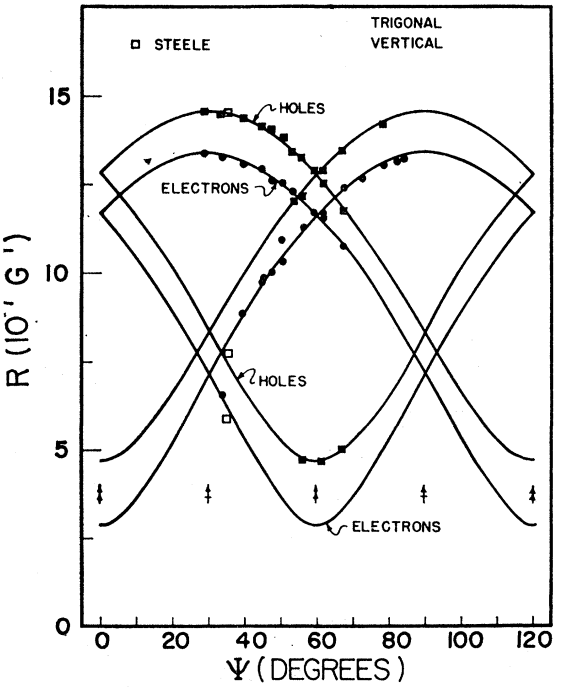

FIG. 5. Period R versus angle ψ where R is the period of the oscillation in $1/H$ with the trigonal axis normal to H and ψ is the angle between the binary and H. The curves are the least-squares fit of Eq. (8).

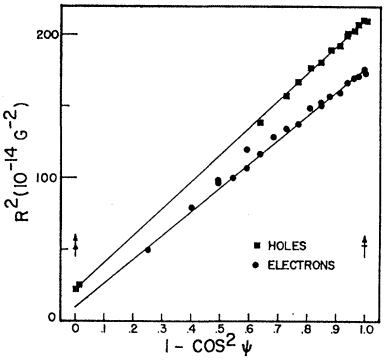

FIG. 6. Plot of R^2 versus $1-\cos^2\psi$ for determination of parameter C. The intercept of the least-squares fitted straight line gives the value of C.

data plotted as R^2 versus $\cos^2\psi$, Fig. 6. The value of A for holes could not be determined; a value 9×10^{-14} G^{-2} was assumed. The experimental values of A, B, C, and D are given in Table I. The curves drawn in Figs. 3–5 are given by Eqs. (6)–(8) for these values.

For the determination of ζ_0, the temperature dependence of the amplitudes (a for electrons, and b for holes) of the oscillations in magnetoresistance, was studied at $\theta=-101.3°$ and $\theta=0°$. At $\theta=-101.3°$, both electrons

TABLE I. Coefficients A, B, C, D for electrons and holes in units of (10^{-14} G^{-2}).

	A	B	C	D
Electrons	101	180	8.4	124
Holes	9.0 (assumed)	212	22	12.7

and holes were observed; at $\theta=0°$, only electrons were observed, see Fig. 3. For a particular carrier, the plot of $\ln(a/T)$ versus T is linear in the first approximation. A slight deviation from linearity of the form $e^{-\lambda/T}$ is expected for λ/T not negligibly small where $\lambda=2\pi^2kT(c/e\hbar\zeta_0)(m^*/H)$. The data were corrected for this nonlinearity, then plotted in Fig. 7. The double-effective Bohr magneton β^* and ζ_0 were computed from the relations

$$\beta^*=2\pi^2k/Hs\,,\qquad \zeta_0=\beta^*/P\,, \tag{9}$$

where s is the slope of the line in Fig. 7. The effective mass was also estimated from

$$m^*=e\hbar/\beta^*c\,. \tag{10}$$

The values of ζ_0 and m^* are given in Table II.

TABLE II. Chemical potential ζ_0 and effective mass m^* for electrons and holes from the temperature dependence of the ρ_{11} oscillation amplitudes.

Orientation θ (deg)	Electrons m^*/m_0	Electrons ζ_0 (10^{-14} erg)	Holes m^*/m_0	Holes ζ_0 (10^{-14} erg)
−101.3	0.082	19.7	0.10	13.0
0	0.09	20.3	...	...

TABLE III. Comparison of $\hat{\alpha}$ tensor elements, chemical potential ζ_0, and density of carriers n for electrons.

Reference	α_{11}	α_{22}	α_{33}	α_{23}	ζ_0 (10^{-14} erg)	n (10^{19} cm^{-3})
Present work	19.1	6.3	11.3	7.8	20.3	4.15
Eckstein[a]	16.7	5.98	11.61	7.54	18.6	...
Datar[b]	20.0[e]	6.05[e]	11.9[e]	7.79[e]	...	...
Shoenberg[c]	20.0	10.0	5.2	6.5	18.0	3.7
Juretschke[d]	...	...	...	...	20.8	4.3

[a] See Ref. 7.
[b] See Ref. 5.
[c] See Ref. 4.
[d] See Ref. 11.
[e] Computed from author's data with $\zeta_0=20.3\times10^{-14}$ erg assumed.

B. Electron Band Structure

The periods P's, Q's, and R's for a three-ellipsoid set of Fermi surfaces describe the electrons quite well as evident in Figs. 3–5. Each ellipsoid is tilted out of the basal plane with its major axis at 36° with respect to the basal plane as seen from period P_1 having a minimum at 36° and a maximum at −54° and period Q_1 having a minimum (extrapolated) at ∼−90°.

The components of the tensor $\hat{\alpha}$ as computed from the data in Tables I and II, the chemical potential ζ_0, and the electron population n as computed from

$$n=(3\pi^2)^{-1}(2e/ch)^{3/2}[C(AB-D^2)]^{-1/4} \tag{11}$$

are given in Table III. For comparison, the previously

TABLE IV. Cyclotron and effective masses for electrons.

	m^*/m_0 Trigonal	m^*/m_0 Binary	m^*/m_0 Bisectrix	Components of effective mass tensor in units of m_0: m_1	m_2	m_3	m_4
Present work	0.090	0.31	0.069	0.052	1.09	0.64	0.75
Eckstein[a]	0.1	...	...	0.6[e]	0.92[e]	0.48[e]	0.6[e]
Datars[b]	0.088±0.005	0.31	0.068	0.05	1.03	0.53	0.67
Shoenberg[c]	0.071[e]	...	...	0.05	1.0	0.52	0.65
Smith[d]	...	...	0.088	...	...	...	...

[a] See Ref. 7.
[b] See Ref. 5.
[c] See Ref. 4.
[d] G. E. Smith, J. K. Galt, and F. R. Merritt, Phys. Rev. Letters, 4, 276 (1960).
[e] Computed from the authors' data.

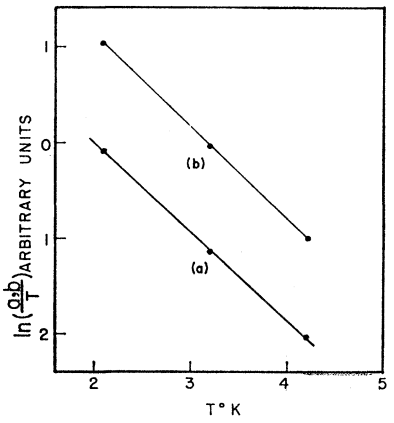

FIG. 7. Plot of $\ln[(a,b)/T]$ versus T for determination of the chemical potential ζ_0 by Eq. (9). (a,b) denote the amplitude of the oscillations at $\theta=-101.3°$ where a is the amplitude for electrons and b for holes.

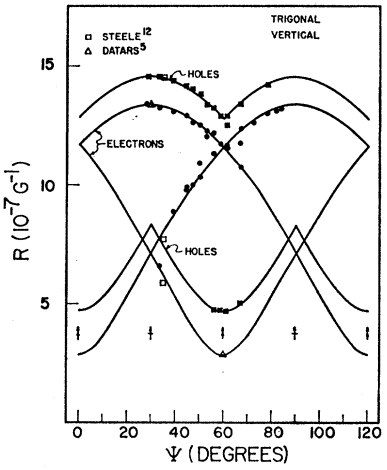

FIG. 8. Alternate scheme for the hole Fermi surface. Compare with Fig. 5.

reported values are also given in Table III. The agreement is good.

The cyclotron masses are computed from the relation

$$m^* = (e\hbar/c)/\zeta_0 \Delta(1/H), \qquad (12)$$

where $\Delta(1/H)$ is the period in $1/H$ of the appropriate oscillation; these results are given in the first three columns of Table IV. The components of the effective mass tensor as obtained from the inversion of the $\hat{\alpha}$ tensor are given in the last four columns of the table. The agreement between the present results and those in the literature is evident from Table IV.

C. Hole Band Structure

With the assumption of a three-ellipsoid set of Fermi surfaces for holes analogous to those for electrons, corresponding results for the $\hat{\alpha}$ tensor elements, chemical potential, carrier density, and cyclotron and effective masses are obtained for holes, see Tables V and VI. All that can be deduced from comparison with the scanty amount of previously reported data is that the present results are reasonable.

The curves labeled "holes" drawn in Figs. 3–5 are the analytic results of the three-ellipsoid Fermi surface assumption for the present experimental values of A, B, C, and D. As evident, the available data points fit the curves well; however, the number of data points is not

TABLE V. Comparison of $\hat{\alpha}$ tensor elements, chemical potential ζ_0, and density of carriers n for holes.

	α_{11}	α_{22}	α_{33}	α_{23}	ζ_0 (10^{-14} erg)	n (10^{19} cm^{-3})
Present work	6.0	0.7	17.3	1.0	13.0	3.80
Datars[a]	...	...	...	...	...	...
Juretschke[b]	...	...	...	...	9.6	4.3
Freedman[c]	...	...	...	...	...	3.7

[a] See Ref. 6.
[b] See Ref. 11.
[c] See Ref. 10.

TABLE VI. Cyclotron and effective masses for holes.

	m^*/m_0			Components of effective mass tensor in units of m_0			
	Trigonal	Binary	Bisectrix	m_1	m_2	m_3	m_4
Present work	0.48	0.11 0.303	0.098	0.154	1.47	0.06	0.006
Datars[a]	0.32 ±0.02 0.11 ±0.005	...	...	...	...	...	...
Juretschke[b]	0.34	...	...	...	...	...	...

[a] See Ref. 6.
[b] See Ref. 11.

sufficient to define the curves. Figure 3 has no data points in the lower "holes" curve; Fig. 4, no points on the lower "holes" curve for $0<\theta\lesssim 80°$; and Fig. 5 contains so few data that an alternate set of "holes" curves are possible, for example, those drawn in Fig. 8.

The "holes" curves in Figs. 3–5 correspond to ellipsoidal surfaces shown schematically in Fig. 9(a). The alternative curves shown in Fig. 8 correspond to surfaces shown in Figs. 9(b)–9(d). These surfaces are those of a two-band model with one band being actually two, almost degenerate bands. The large mass band is that of the "star" surface of Fig. 9(b); the two, almost degenerate bands, are those of the "triangle" surfaces in Figs. 9(c) and 9(d). The relation of these surfaces to the ellipsoidal ones considered in the foregoing is best understood from careful comparison of Figs. 9(a)-9(d). A

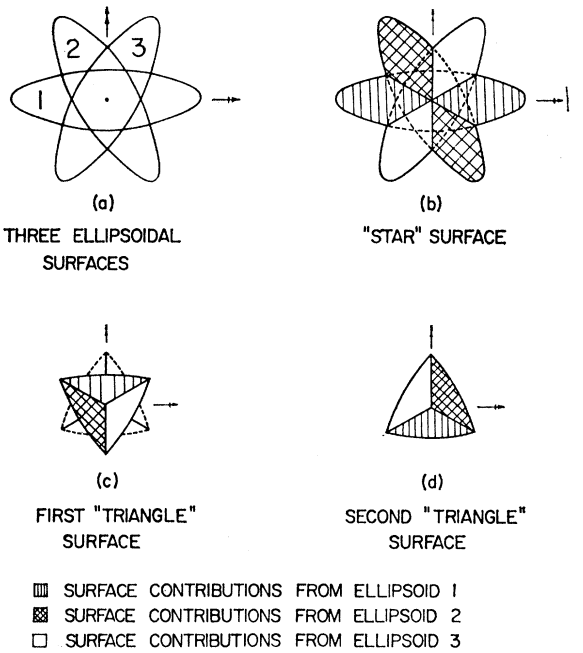

FIG. 9. (a) Three ellipsoid Fermi surface model such as would give holes' curves in Fig. 5. (b) "Star" Fermi surface as formed essentially from portions of the three ellipsoidal surfaces. This surface would result in the lower holes' curve in Fig. 8. (c) and (d) "Triangle" Fermi surfaces as formed from portions of the three ellipsoidal surfaces. These surfaces are degenerate and would result in the upper holes' curve in Fig. 8.

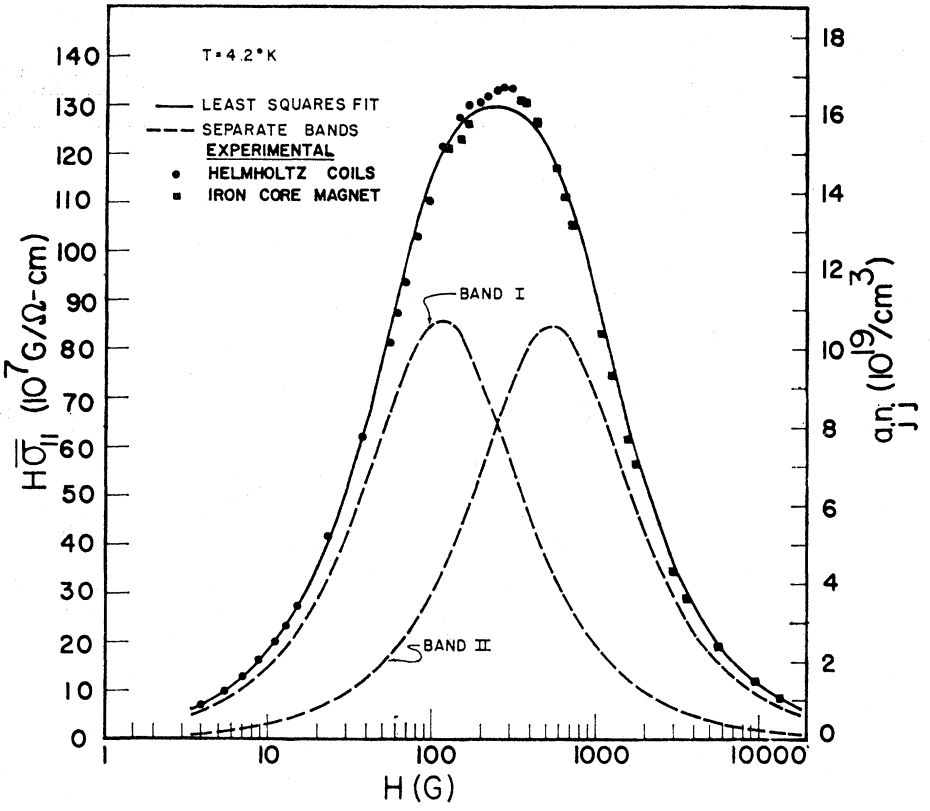

FIG. 10. $H\bar{\sigma}_{11}$ versus H for $T=4.2$°K. Solid curve is least-squares fit for a two band, the dotted curves being the individual band contributions.

third possibility is the replacement of the two "triangle" surfaces by another "star." The present data do not warrant further discussion of these possibilities. However, one of these alternate band structures may furnish an explanation for the two cyclotron masses for holes found by Datars.[6]

III. STUDY OF THE MAGNETIC FIELD DEPENDENCE OF THE NONOSCILLATORY PARTS OF THE ELECTRICAL CONDUCTIVITIES

A. Experimental Results

The coefficients of magnetoresistance ρ_{11} and Hall-resistance ρ_{21} were measured with the current in the

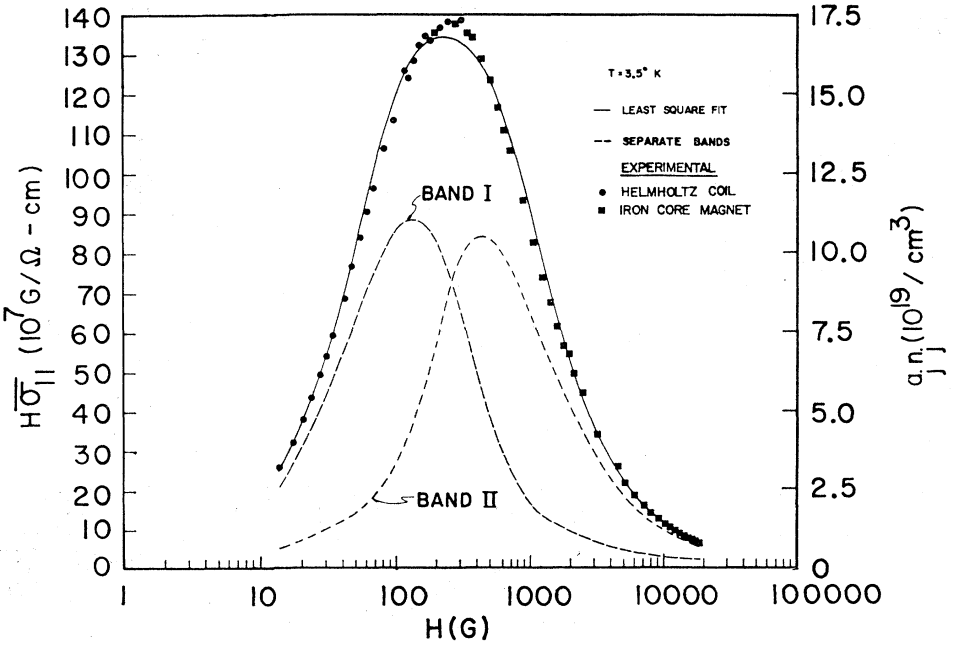

FIG. 11. $H\bar{\sigma}_{11}$ versus H for $T=3.5$°K. Solid curve is least-squares fit for a two band, the dotted curves being the individual band contributions.

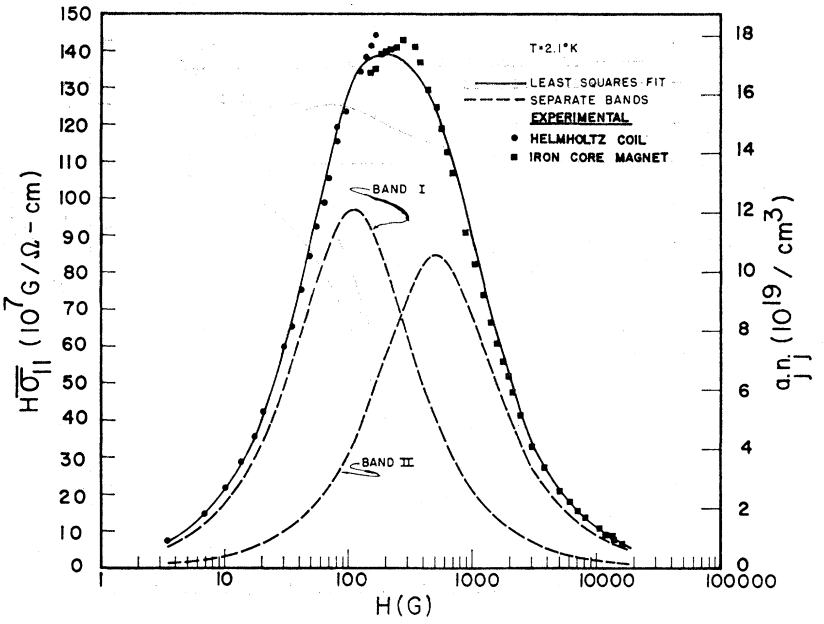

FIG. 12. $H\bar{\sigma}_{11}$ versus H for $T=2.1$°K. Solid curve is least-squares fit for a two band, the dotted curves being the individual band contributions.

binary direction and the magnetic field along the trigonal axis. The corresponding elements of the conductivity tensor were computed as

$$\sigma_{11}=\rho_{11}/(\rho_{11}^2+\rho_{21}^2)$$
$$\sigma_{12}=\rho_{21}/(\rho_{11}^2+\rho_{21}^2), \tag{13}$$

where σ_{11} and σ_{12} are the magnetoconductivity and the Hall conductivity, respectively. The nonoscillatory parts of σ_{11} and σ_{12}, denoted as $\bar{\sigma}_{11}$ and $\bar{\sigma}_{12}$, respectively, were separated from the oscillatory parts and the quantities $H\bar{\sigma}_{11}$ and $\bar{\sigma}_{12}$ plotted versus log$H$. The data for $H\bar{\sigma}_{11}$ at temperatures 4.2, 3.5, 2.1, and 1.7°K are given in Figs. 10–13; the data for $\bar{\sigma}_{12}$ at the same temperatures, in Figs. 14–17. The experimental arrangement used a set of Helmholtz coils for fields less than 100 G and an iron-core electromagnet for fields greater than 100 G; the scatter in data around 100 G in Figs. 10–17 is the unfortunate results of this change in experimental conditions.

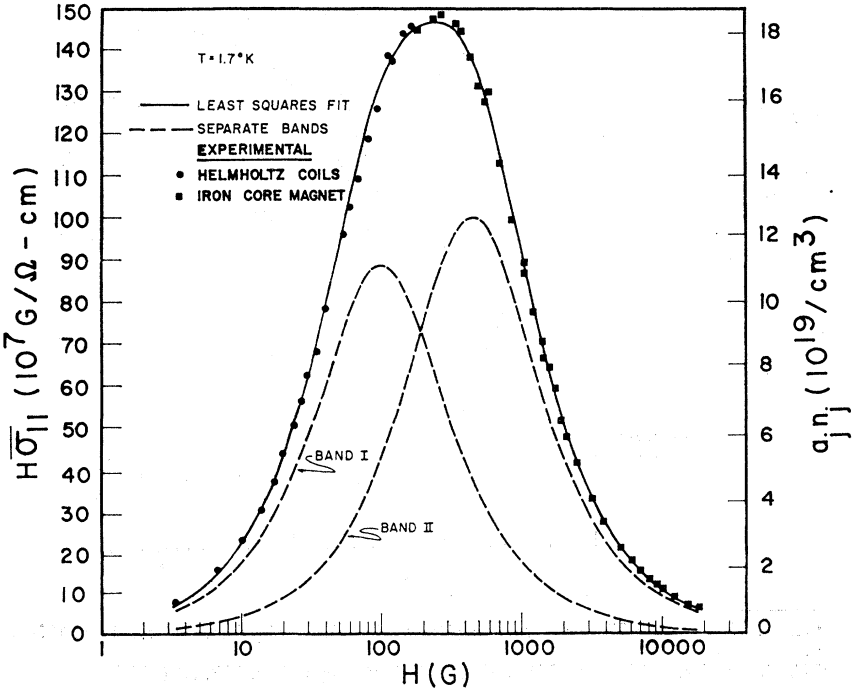

FIG. 13. $H\bar{\sigma}_{11}$ versus H for $T=1.7$°K. Solid curve is least-squares fit for a two band, the dotted curves being the individual band contributions.

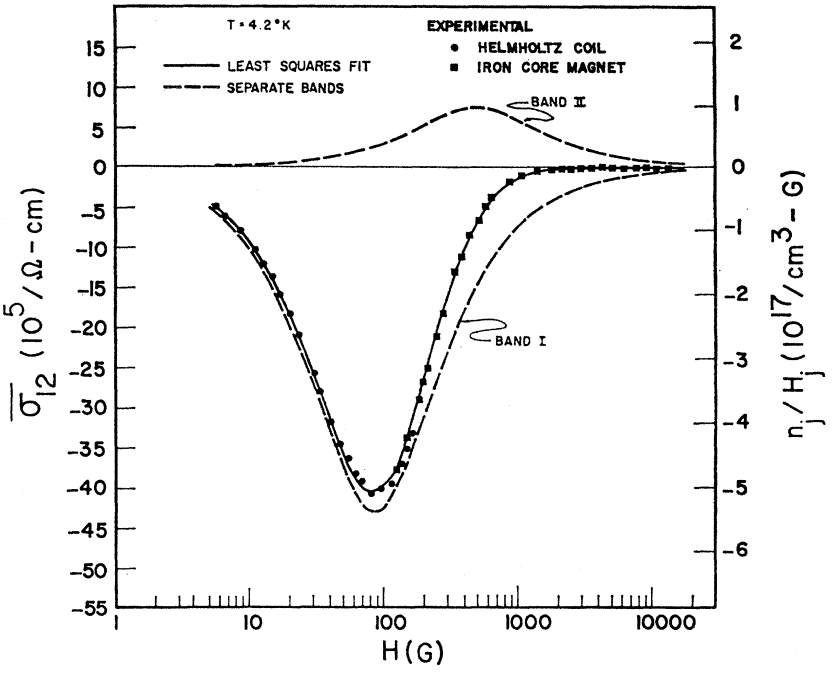

FIG. 14. $\bar{\sigma}_{12}$ versus H for $T=4.2$°K. Solid curve is least-squares fit for a two band, the dotted curves being the individual band contributions.

B. Analysis

The non-oscillatory parts of the conductivities are given in the Sondheimer-Wilson[14,15,16] theory as

$$\bar{\sigma}_{11}=ec\sum a_j n_j H_j L_j\,,$$
$$\bar{\sigma}_{12}=ec\sum(\pm)n_j L_j H\,, \tag{14}$$

where the subscripts denote the carrier band and the summation is over all bands. The $(\pm)$ symbol in $\bar{\sigma}_{12}$ indicates that the sign for each term is taken appropriate to the charge of the carrier. The quantities in the above are defined as follows:

(1) The factor a_j is an adjustable parameter intro-

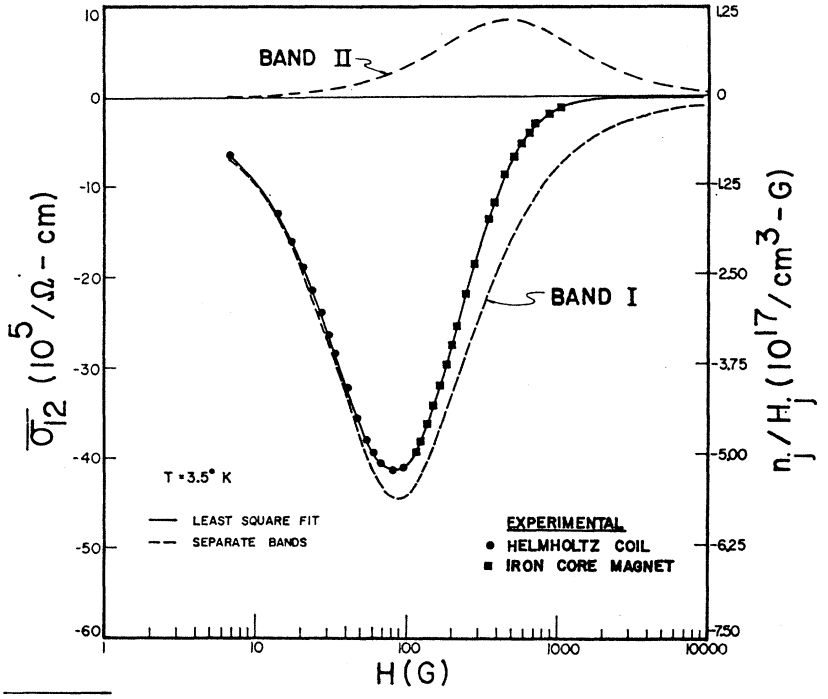

FIG. 15. $\bar{\sigma}_{12}$ versus H for $T=3.5$°K. Solid curve is least-squares fit for a two band, the dotted curves being the individual band contributions.

[14] A. H. Wilson, *The Theory of Metals* (Cambridge University Press, Cambridge, 1954).
[15] See Ref. 3.
[16] C. G. Grenier, J. M. Reynolds, and J. R. Sybert, Phys. Rev. **132**, 58 (1963).

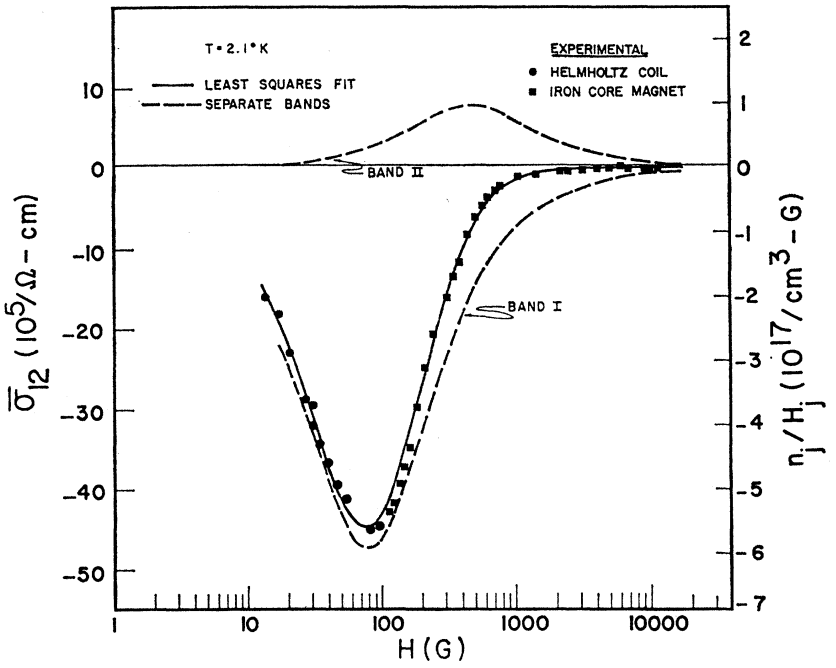

FIG. 16. $\bar{\sigma}_{12}$ versus H for $T=2.1$°K. Solid curve is least-squares fit for a two band, the dotted curves being the individual band contributions.

duced to account for noncircular orbits of the carriers; a_j equals one for circular orbits and can be expressed in terms of the $\hat{\alpha}$ tensor elements as

$$a_j=\tfrac{1}{2}[(\alpha_{11}/\alpha_{22})^{1/2}+(\alpha_{22}/\alpha_{11})^{1/2}].$$

(2) H_j is the saturation field defined as

$$H_j=cm_j^*/e\tau_j,$$

where τ_j is the relaxation time in the jth band; and

(3) L_j is the Lorentz factor

$$L_j=(H^2+H_j^2)^{-1}.$$

Equation (14) is a good approximation for low field results but it is of interest to study its validity over the whole range of field covered in the present experiment.

Two bands were assumed and the data fitted by a least-squares technique.[17] The mean error of the fit was less than 5%. Attempts to use more than two bands for the curve fitting were unsuccessful as the iterative process diverged rapidly. The values of a_jn_j and H_j obtained from the $\bar{\sigma}_{11}$ data are given in the Table VII; the dotted curves drawn in Figs. 10–13 show the contributions of the individual bands and the solid curve, the sum of the two. The values of n_j and H_j obtained from

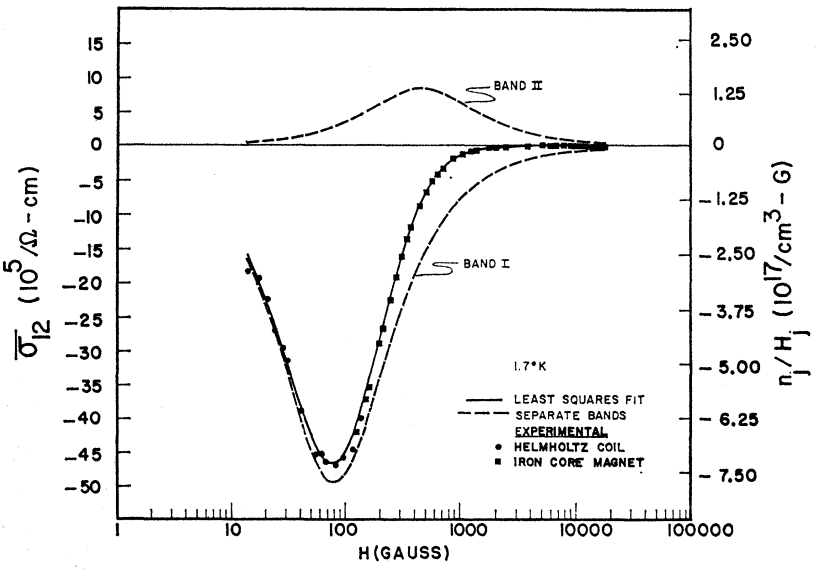

FIG. 17. $\bar{\sigma}_{12}$ versus H for $T=1.7$°K. Solid curve is least-squares fit for a two band, the dotted curves being the individual band contributions.

[17] H. J. Mackey, Ph.D. dissertation, Louisiana State University, 1963 (unpublished).

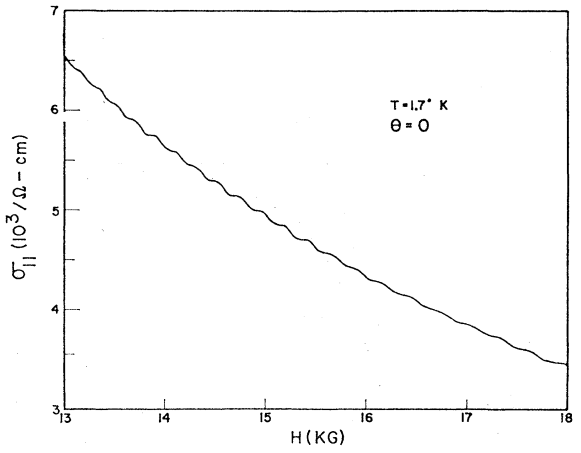

FIG. 18. Oscillations in σ_{11} at $T=1.7$°K at $\theta=0$.

the $\bar{\sigma}_{12}$ data are given in Table VIII; the dotted curves in Figs. 14–17 are the contributions of the individual bands and the solid curve the sum. In these, the subscripts 1 denote the electron band and subscripts 2, the hole band. This follows from the fact that $H_2/H_1 \simeq 5$, that is, approximately equal to the ratio of the cyclotron mass (in the trigonal direction) of the carriers identified as holes to that of the carriers identified as electrons, see Sec. II.

There is an evident disagreement between the H_j determined from the $\bar{\sigma}_{11}$ data and that from the $\bar{\sigma}_{12}$ data. A second difficulty is that a_1 and a_2 computed from these data are 2.0 and 2.5, respectively; but the α's data of Sec. II give $a_1=1.1$ and $a_2=1.7$. These differences are not surprising in view of the great idealization of the Sondheimer-Wilson theory; inclusion of such effects as anisotropy and/or magnetic field dependence of τ_j and m_j^* could readily account for the discrepancies.

A simultaneous fit to both the $\bar{\sigma}_{11}$ and $\bar{\sigma}_{12}$ data at 4.2°K gave the following values:

$$n_1=5.05\times10^{19}\ \text{electrons/cm}^3,$$
$$n_2=5.05\times10^{19}\ \text{holes/cm}^3,$$
$$a_1n_1=8.1\times10^{19}/\text{cm}^3,$$
$$a_2n_2=13.2\times10^{19}/\text{cm}^3,$$
$$a_1=1.6,$$
$$a_2=2.6,$$
$$H_1=90.7\ \text{G},$$
$$H_2=467\ \text{G}.$$

The mean error in the simultaneous fit was about twice that of the individual fits.

The temperature dependencies of the H_j, n_j, and a_j seem strange. Particular attention is directed to the fact that the H_j determined from $\bar{\sigma}_{11}$ has a temperature dependence different than that of the H_j determined from $\bar{\sigma}_{12}$. These effects also indicate some inadequacy of the Sondheimer-Wilson theory for detailed treatment of antimony arising probably from the extension of this theory to high field.

TABLE VII. a_{jnj} and H_j as determined from $\bar{\sigma}_{11}$ and a_j as determined from both $\bar{\sigma}_{11}$ and $\bar{\sigma}_{12}$.

T (°K)	a_1n_1 (10^{19}/cm³)	H_1 (G)	a_1	a_2n_2 (10^{19}/cm³)	H_2 (G²)	a_2
4.2	10.7	115	2.27	10.6	540	2.28
3.5	11.5	115	2.31	10.4	531	2.11
2.1	12.2	110	2.58	10.5	512	2.24
1.7	11.3	101	2.28	12.4	453	2.52

IV. STUDY OF THE SHUBNIKOV-DE HAAS OSCILLATION AMPLITUDES

A. Experimental Results

Pronounced Shubnikov-de Haas oscillations were observed in the conductivities σ_{11} and σ_{12}, see Figs. 18 and 19. The oscillations were studied with the field along the trigonal axis for fields between 13 and 18 kG. The data seem to indicate more than one periodic component, especially in σ_{11}. These components were not resolved but at least the contributions of two roughly equal periods seem to be present.

The amplitudes of the oscillations were measured and are given in Table IX.

B. Analysis

Attempts have been made to produce a theory of the Shubnikov-de Haas oscillations, first by Levinger and Grimsal,[18] and later by Lifshitz and Kosevich.[19] These considered the effects of field-dependent variations in carrier densities and Fermi energies of the carrier bands. Zil'berman[20] and others[21] considered effects of Landau quantization on the mobility of the carriers. A short summary of these theories is given in present notation by Grenier, Reynolds, and Sybert.[16]

In the particular case of two bands with equal carrier densities, the Lifshitz-Kosevich theory under some simplifying assumptions[17] gives the amplitude of $\bar{\sigma}_{\alpha\beta}$,

TABLE VIII. n_j and H_j as determined from $\bar{\sigma}_{12}$.

T (°K)	n_1 (10^{19}/cm³)	H_1 (G)	n_2 (10^{19}/cm³)	H_2 (G)
4.2	4.71	86.4	4.65	492
3.5	4.95	86.8	4.95	457
2.1	4.71	79.2	4.70	473
1.7	4.93	79.6	4.93	459

[18] J. S. Levinger, E. G. Grimsal, Phys. Rev. **94**, 772 (1958).
[19] I. Lifshitz and L. M. Kosevich, Zh. Eksperim. i Teor. Fiz. **33**, 88 (1957) [translation: Soviet Phys.—JETP **6**, 67 (1958)].
[20] G. E. Zil'berman, Zh. Eksperim. i Teor. Fiz. **29**, 762 (1955) [translation: Soviet Phys.—JETP **2**, 650 (1956)].
[21] List of references is given in the review article by A. H. Kahn and P. R. Frederikse in *Solid State Physics*, edited by F. Seitz and P. Turnbull (Academic Press Inc., New York, 1960), Vol. 9.

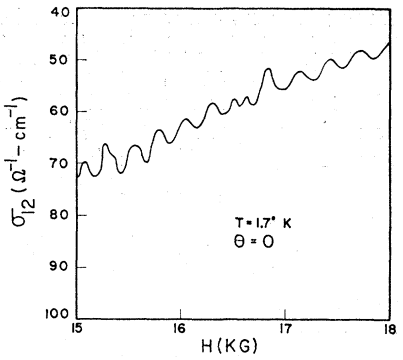

FIG. 19. Oscillations in σ_{12} at $T=1.7°K$ at $\theta=0$.

the oscillatory part of $\sigma_{\alpha\beta}$ due to the first band as

$$\tilde{\sigma}_{\alpha\beta}|_{\text{L-K}}=\bar{\sigma}_{\alpha\beta}\zeta_1(\zeta_1+\zeta_2)^{-1}|\tilde{n}/n|, \quad (15)$$

where the ζ's are the Fermi energies and $|\tilde{n}|$, the amplitude of the variations in carrier density, is to lowest order in λ

$$|\tilde{n}/n|=(\tfrac{3}{2}\pi)(\tfrac{1}{2}PH)^{3/2}\lambda(\sinh\lambda)^{-1}\cos(\pi m^*/m_0),$$

with P the period in H^{-1} of the oscillation and

$$\lambda=2\pi^2kT\zeta_0^{-1}(PH)^{-1}.$$

The Zil'berman theory gives the amplitude of $\tilde{\sigma}_{11}$ for the present case and with $\tilde{\sigma}_{11}$ defined by Eq. (14)

$$\tilde{\sigma}_{11}|_{\text{ZII}}=\bar{\sigma}_{11}a_1H_1(a_1H_1+a_2H_2)^{-1}\times(5\sqrt{2}/4)(PH)^{1/2}\lambda(\sinh\lambda)^{-1}. \quad (16)$$

This contribution arises from the first band only, effects of the second band being relatively small. Within the present approximation, the Zil'berman theory differs from the Lifshitz-Kosevich theory primarily in the (PH) dependence.

Amplitudes computed from Eqs. (15) and (16) are given in Table IX. Clearly the values given by the Lifshitz-Kosevich theory are too small by one-to-two orders of magnitude. The results of Zil'berman theory agree in order of magnitude with the experimental data as shown in Table IX.

V. CONCLUSION

The results of the present study of galvanomagnetic effects and band structure of antimony are summarized as follows:

(i) The electron Fermi surface as mapped from the dependence of the Shubnikov-de Haas oscillations on crystal orientation is in good accord, within experimental error, with previous studies. The results showed the tilted three-ellipsoid model of Shoenberg to be satisfactory for electrons. The determination of the hole Fermi surface was ambiguous because the periods at certain orientations of the crystal with respect to the magnetic field could not be measured. The data were compatible not only with a three-ellipsoid Fermi surface but with more complicated shapes as well.

TABLE IX. Amplitudes of Shubnikov-de Haas oscillations.

H (kG)	$\tilde{\sigma}_{11}\|_{\text{exp}}$ (Ω^{-1}-cm^{-1})	$\tilde{\sigma}_{12}\|_{\text{exp}}$ (Ω^{-1}-cm^{-1})	$\tilde{\sigma}_{11}\|_{\text{L-K}}$ (Ω^{-1}-cm^{-1})	$\tilde{\sigma}_{12}\|_{\text{L-K}}$ (Ω^{-1}-cm^{-1})	$\tilde{\sigma}_{11}\|_{\text{ZII}}$ (Ω^{-1}-cm^{-1})
17.8	16.6	~1	0.64	9.1×10^{-3}	56
16.9	17.2	···	0.64	9.5×10^{-3}	45
15.9	26.1	···	0.64	1.0×10^{-2}	37
14.8	36.8	···	0.63	1.1×10^{-2}	29
13.6	24.3	···	0.62	1.2×10^{-2}	22

(ii) The nonoscillatory parts of the conductivities were analyzed on the basis of the Sondheimer-Wilson theory for a two-band model. Data for each conductivity tensor element were fitted separately and accurately; however, the separate fits gave rise to slightly different saturation fields for the different conductivity elements. In addition, these data produced values for carrier orbit shape parameters in disagreement with the values obtained in the Shubnikov-de Haas oscillations study. The discrepancies are attributed to the Sondheimer-Wilson theory being too great an idealization for detailed application to antimony.

(iii) The densities of electron and hole carriers were found to be equal but with the electron mobility in the binary direction five times that of the holes (H parallel to the trigonal direction).

(iv) The amplitude of Shubnikov-de Haas oscillations was found to be much larger in σ_{11} than in σ_{12}. These amplitudes are one-to-two orders of magnitude larger than explainable by the Lifshitz-Kosevich theory but are in order-of-magnitude agreement (for σ_{11} only) with the Zil'berman theory.

ACKNOWLEDGMENT

We are indebted to Dr. J. D. Childress for useful discussions, and to Dr. H. J. Mackey for making his IBM programs available.

APPENDIX: EXPERIMENTAL DETAILS

The single crystal of antimony was grown by a modified Bridgman technique[22,23] in a helium atmosphere. The antimony ingot, from which the crystal was prepared, was obtained from Johnson Matthey and Company, Ltd.

The single crystal obtained was cleaved in the basal plane at room temperature and was cut with a spark cutter[24] under kerosene. The final size of the crystal was 10 mm×2 mm×2 mm. The back reflection Laue photographs showed no signs of strain in the crystal. The crystallographic axes with respect to the specimen dimensions are shown in the Fig. 2. The ratio $R_{300°K}/R_{4.2°K}$ was found to be 720.

The specimen was mounted on a Lucite holder, directly in contact with liquid helium. This arrangement

[22] P. W. Bridgman, Proc. Am. Acad. Arts Sci. **60**, 305 (1925).
[23] D. S. Balain, Dissertation, Louisiana State University, 1960 (unpublished).
[24] B. S. Chandrasekhar, Rev. Sci. Instr. **32**, 368 (1961).

also ensures the isothermal conditions under which this experiment was done. The connections for current and potential leads were made with No. 34 Formvar insulated copper wire soldered with (Bi-Cd) eutectic mixture.[25]

The Dewar flask for liquid helium was described elsewhere.[26] The potentials were measured with a Rubicon potentiometer, the off-balance of which was recorded on a Brown Recorder after amplification with a low-impedance Becker D. C. Amplifier. The currents passed through the crystal were of the order of 500 mA in the low field and 50 mA in the high field.

The electromagnet, for the field range of 130 G to 18 kG was an iron core Weiss magnet with 8-in.-diam pole pieces separated by $1\frac{5}{8}$-in. air gap. It could be rotated through 360° about its vertical axis. The calibration of the field was made with a nuclear resonance Gaussmeter.

For the lower ranges of the field,[27] a pair of Helmholtz coils were used which were calibrated with a ballistic galvanometer.

[25] Colin J. Smithells, *Metal Reference Book* (Interscience Publishers, Inc., New York, 1955), 2nd ed., Vol. 11, p. 959.

[26] J. R. Sybert, Dissertation, Louisiana State University, 1963 (unpublished).

[27] R. J. Gillingham, S. J., Dissertation, Louisiana State University, 1963 (unpublished).